Original Paper

A multi-method characterization of borosilicate glasses doped with 1 up to 10 mol% of Fe, Ti and Sb

Adelheid Schütz and Doris Ehrt

Otto-Schott-Institut für Glaschemie, Friedrich-Schiller-Universität Jena, Jena (Germany)

Manfred Dubiel and Xiuchung Yang

Physikalische Fakultät, Martin-Luther-Universität Halle-Wittenberg, Halle (Germany)

Bernd Mosel and Hellmut Eckert

Institut für Physikalische Chemie, Westfälische Wilhelms-Universität Münster, Münster (Germany)

The model glasses NBS1 and NBS2 are sodium borosilicate glasses of high intrinsic UV transmission. Although both glasses have an SiO_2 content of 74 mol%, they possess different matrix structures due to varied Na_2O / B_2O_3 ratios. Nonbridging oxygens occur in the NBS1 but not in the NBS2 glass.

Fe, Ti and Sb oxides were added at concentrations of 1 and 10 mol% to study valence, coordination and site distribution. XANES, Mössbauer, optical absorption, photoluminescence and EPR spectroscopy provided an insight into the structures and near range environments of the dopants.

Large differences were found for the two Fe doped glasses. The presence of nonbridging oxygens in NBS1 glass leads to a higher solubility of the Fe ions and a higher ratio of tetrahedral over octahedral Fe^{3+} coordination while a clustering of Fe ions resulting in a lowered UV and VIS transmission is observed in NBS2 glass. In Ti doped glasses EPR and XANES spectroscopy shows that most Ti occurs as Ti^{4+}, in four-, five- and sixfold coordination. Optical spectra of Ti^{4+} display high intensity charge transfer transitions in the UV region. Ti^{4+} photoluminescence in the visible range is of low intensity.

Optical absorption, XANES and Mössbauer spectroscopy could only detect Sb^{3+} in the antimony doped glasses. The photoluminescence of Sb^{3+} is much stronger in the NBS1 than in the NBS2 glass.

1. Introduction

Borosilicate glasses offer favourable material properties such as chemical resistance, mechanical strength, thermal shock resistance and high optical transmission. They are used for various technical applications and in optical instruments. The properties of sodium borosilicate glasses with a constant SiO_2 content are related to the substructures of the glass matrix such as BO_3, and BO_4 units as well as nonbridging oxygens. The distribution of these entities depends on the Na_2O / B_2O_3 ratio. Nonbridging oxygens are thought to occur only at Na_2O / B_2O_3 ratios > 0.2 [1] and induce a rise in the optical basicity, a measure of the electron donor power, as defined by Duffy [2]. Solarization (radiation induced absorbance and formation of colour centres) is less effective in glasses without nonbridging oxygens [3]. Nonbridging oxygens and different matrix structures influence valence, coordination and site distribution of polyvalent elements incorporated in glasses.

Received 10 February, revised manuscript 20 October 2004.

In order to investigate this influence, two glasses with a constant SiO_2 content of 74 mol% and varied Na_2O / B_2O_3 ratios have been melted and characterized (table 1). Both are simplified models of similar type as BK7® (NBS1) and Duran® (NBS2) borosilicate glasses. NBS1 glass, with a Na_2O / B_2O_3 ratio of 1.6 contains a significant number of nonbridging oxygens and 4 / 5^{th} of all boron is tetrahedrally coordinated by oxygen atoms [4]. NBS2 glass, on the other hand, with an Na_2O / B_2O_3 ratio of 0.2, has hardly any nonbridging oxygens, is characterized by a lower optical basicity than NBS1 glass and most boron is present in trigonal BO_3 units [4]. Those planar boron groups show two different arrangements, isolated in the matrix or connected to boroxol rings [4].

Polyvalent elements are present in most glasses. They are introduced as dopants to alter material properties such as glass colour, as fining agents or they occur as (trace) impurities. Fe ions affect colour, transmission, solarization and may cause phase separation and crystallization in glasses when added at high concentrations [5]. Fe is present in

Table 1. Composition and physical properties of the model glasses studied [4 and 8]

	NBS1	NBS2
composition in mol%:		
SiO_2	74	74
Na_2O	16	4.3
B_2O_3	10	20.7
Al_2O_3	-	1
physical properties:		
T_g in °C	550	440
$\alpha_{100\text{ to }300\,°C}$ in 10^{-7} K^{-1}	88	35
n_e / v_e	1.51 / 63	1.47 / 65
ρ in g / cm³	2.45	2.18
nonbridging oxygens	yes	no
coordination of boron by ^{11}B-NMR (error ± 2 %) [4]	80 % BO_4 - 20 % BO_3	37 % BO_3[1] - 46 % BO_3[2] - 17 % BO_4
optical basicity, according to Duffy [2]	0.56	0.52
impurities Fe and Ti in ppm	3 and 4	1.5 and 3
UV edge λ_0 in nm for 0.2 mm sample	200	170

[1] In boroxol ring structures.
[2] Isolated entities of unknown bonding.

glasses as Fe^{2+} and Fe^{3+}, both ions are found in tetrahedral and octahedral coordination, depending on glass type and concentration [5]. Titanium is used for optical glasses with a high refractive index [6] and UV radiation resistance [3]. Titanium is also one of the most important trace impurities in pure silica and lowers the UV transmission in optical glasses. The redox equilibrium of titanium in silicate glasses favours the +4 over the +3 oxidation state [7 and 8]. Ti^{3+} is always found in octahedral coordination although the degree of distortion varies in different matrices [7 and 9]. Ti^{4+} may adopt tetrahedral, octahedral and square-pyramidal coordination [10]. Antimony is employed as a fining agent. Sb was found to occur in the oxidation states +3 and +5 in silicate glasses [11].

Therefore, the manner in which these common ions are built into glasses is of scientific interest. The energy position, intensity and half widths of their electronic transitions are influenced by the surrounding glass matrix, therefore, electronic transitions are used to derive the actual local structures.

Since the stated matrix structures should affect valence, coordination and site distribution of polyvalent elements, those elements may be used as sensors for glass matrix structures [2 and 12]. The determination of the optical basicity on the basis of the shift of the p→s transition of doped Pb^{2+} is a typical example [2]. A strong influence of the NBS1 and NBS2 glass matrices on the coordination behaviour of Co^{2+} ($3d^7$) and Ni^{2+} ($3d^8$) was also shown in a former project [13]. Since Fe and Ti ions have comparable radii, it was believed they should show distinctive coordination modes in both glass types as well.

In the frame of an ongoing, broader research project, the valence, coordination and site distribution of Fe, Ti, Sb, Sn and Pb ions in two sodium borosilicate glasses are being investigated by combining different analytical methods. The methods used, like optical absorption, photoluminescence, EPR, EXAFS / XANES and Mössbauer spectroscopy, are based on different measuring principles and thus offer different information on the dopants. The different analytical methods vary in their sensitivities and detection limits. Hence, the stated polyvalent elements were doped into the glasses at concentrations ranging between 0.001 and 10 mol%. Results for glasses doped with 1 and 10 mol% of Fe, Ti and Sb ions are presented in this paper.

2. Experimental procedures

2.1 Glass preparation

Both NBS1 and NBS2 glass are made of 74 mol% SiO_2. The compositions of the two different glass types are summarized in table 1. The glass samples were prepared using special high purity grade chemicals with an iron content <1 ppm. The ternary composition of the NBS2 glass tends to liquid-liquid phase separation at higher temperatures [1, 5 and 14]. Thus, 1 mol% Al_2O_3 was added to ensure homogeneous glass formation. Dopants such as Fe_2O_3, FeC_2O_4 and $FeC_4H_4O_6$, TiO_2, Ti_2O_3 and Sb_2O_3 were added to the batch for the preparation of doped glasses. For those samples where reduction of the dopant was desired, the dopant was used in its lower oxidation state along with graphite powder. Batches between 100 and 300 g of glass were mixed and melted in an air atmosphere in a resistance heated electric furnace. Depending on the temperature and components, Pt or Pt-Rh crucibles were employed. Silica glass crucibles were used for all reducing melts. NBS1 glass was melted at 1500 °C and NBS2 glass between 1600 and 1800 °C. The crucibles were removed from the furnace after approximately 2 h. Both glasses were then quenched in water to improve homogeneity and remelted at the same temperature for another 2 h, except for the reducing melts that simply remained in the oven for 4 h. The melts were then poured into a preheated graphite mould and transferred to an annealing furnace where they cooled to room temperature with a cooling rate of about 30 K / h after being held for 30 min at 600 and 500 °C, for NBS1 and NBS2 glass, respectively.

Table 2. XANES results for Fe containing samples and reference substances

sample	K-edge in eV	pre-edge in eV	
		position	height
Fe foil (Fe^0, body centred cubic lattice)	7107.2	none	none
Fe_2O_3 (Fe^{3+} O_h, T_d)	7112.6	7103.6	0.08
Fe_3O_4 (Fe^{3+} O_h, T_d; Fe^{2+} O_h)	7110.8	7102.5	0.09
NBS1/1% Fe	7111.9	7102.9	0.10
NBS1/1% Fe/red	7107.2	none	none
NBS1/10% Fe	7112.7	7103.6	0.12
NBS1/10% Fe/red	7109.4	7102.0	0.064
NBS2/1% Fe	7111.4	7102.9	0.10
NBS2/10% Fe	7112.3	7103.5	0.10
NBS2/10% Fe/red	7110.8	7103.4	0.078

2.2 Spectral characterization

The XANES measurements at the Ti K-edge (4966 eV) and Fe K-edge (7112 eV) were collected at the positron storage ring DORIS III at the beam line E4 of HASYLAB in Hamburg (Germany). An Si (111) double-crystal monochromator was used with an energy resolution of $\Delta E_n / E_n \cong 2.5 \times 10^{-4}$. The experiments were performed in transmission mode at room and liquid nitrogen temperature. Harmonic rejection was achieved by detuning the monochromator crystals between 40 and 50 %. The X-ray intensities were measured with ionization chambers. Ti and Fe foils were used as standards for data analysis. Other samples measured for reference purposes were the crystalline compounds of TiO_2 (and $Ba_2TiSi_2O_8$, $BaTiO_3$, Ba_2TiO_4, Ti_2O_3) and Fe_2O_3 (and Fe tartrate, Fe oxalate, Fe_3O_4, $Fe(NO_3)_3$). Some of these Fe reference substances are included in table 2. The optimum sample concentration was attained by preparing pellets from a mixture of powdered glasses with polyethylene.

^{57}Fe and ^{121}Sb Mössbauer spectra were recorded using a linear arrangement of source, absorber and NaI(Tl) scintillation detector. Sb absorbers were cooled to 78 K using a bath cryostat (MD 300, Oxford). The sources $^{57}Co/Rh$ (Wissel) and $Ba^{121}SnO_3$ (NEN) were always kept at room temperature. The velocity scale of iron was calibrated by laser interferometer and that of antimony by Mössbauer spectra of α-iron. Isomer shift values of iron and antimony are quoted relative to α-iron and to the antimony source, respectively. The experimental data were fitted to different Mössbauer sites based on theoretically calculated line shapes arising from the allowed transitions between ground and excited nuclear states.

UV visible near IR spectra were measured using a double beam spectrophotometer (UV-3102, Shimadzu, Tokyo (Japan)), recording the absorption $E = \lg (I_o / I)$, (error < 1 %), which was standardized after background correction to a nominal path length (d) of 1 cm. For photoluminescence spectra a Shimadzu RF-5001 PC spectrometer was employed, both excitation and emission spectra were recorded at ambient temperature in reflection and transmission mode with an intensity error < 10 %. All optical spectra were analysed and fitted with Gaussian bands using customary computer software.

EPR samples consisted of powdered pieces and small polished plates sawn from the same material as the optical samples. The EPR spectra were recorded at the x-band (≈9.8 GHz) at room temperature in a Bruker ESP 300 E spectrometer (Bruker, Karlsruhe (Germany)), using 1.1-diphenyl-2-piterylhydroxyl (DPPH) as spin standard substance. Band separation of the Ti^{3+} and Fe^{3+} spectra was accomplished with WIN-EPR® software by Bruker. Since the spectra were integrated twice, an experimental error of 10 % may occur.

3. Results and discussion

It is noteworthy that the redox ratios given below do not represent equilibrium ratios and cannot be attributed to the influence of the glass basicity alone, since the glasses were melted at different temperatures.

3.1 Valence states of iron – Fe^{3+} ($3d^5$) / Fe^{2+} ($3d^6$) / Fe^0 ($3d^8$)

3.1.1 XANES spectroscopy

Fe-XANES results are summarized in table 2 and shown in figures 1a and b. The position of the XANES edge stands for the valence of the ions, i.e. the redox ratio is reflected in its position on the energy scale. The XANES spectra of the two nonreduced samples with 1 mol% Fe have edge energies that differ by 0.5 eV (table 2), NBS1 glass has a higher ratio of Fe^{3+} / Fe^{2+}. The most striking edge shift occurred in the sample NBS1/1%Fe/reduced (red), where a shift of 5.4 eV, as compared to Fe_2O_3, was observed (figure 1a). The K-edge position is found at the same energy as the Fe^0 reference which indicates that most iron was reduced to Fe^0 as it would be anticipated in silicate glasses melted under strongly reducing conditions [7 and 15]. Fe^0 is incorporated in small spheres into the glass, as was seen by electron microprobe analysis (figure 2).

From EXAFS, the following redox percentages were calculated [16]. 80 % Fe^{3+} and 20% Fe^{2+} of all iron used were found in NBS1/1% Fe and 60% Fe^{3+} and 40% Fe^{2+} in NBS2/1% Fe. Since these glasses had been melted at different temperatures, these values may not depend solely on the glass type. At concentrations of 10 mol% Fe, the Fe^{3+} / Fe^{2+} ratio is slightly increased (table 2, figure 1b) which is reflected by shorter average bond lengths calculated from EX-

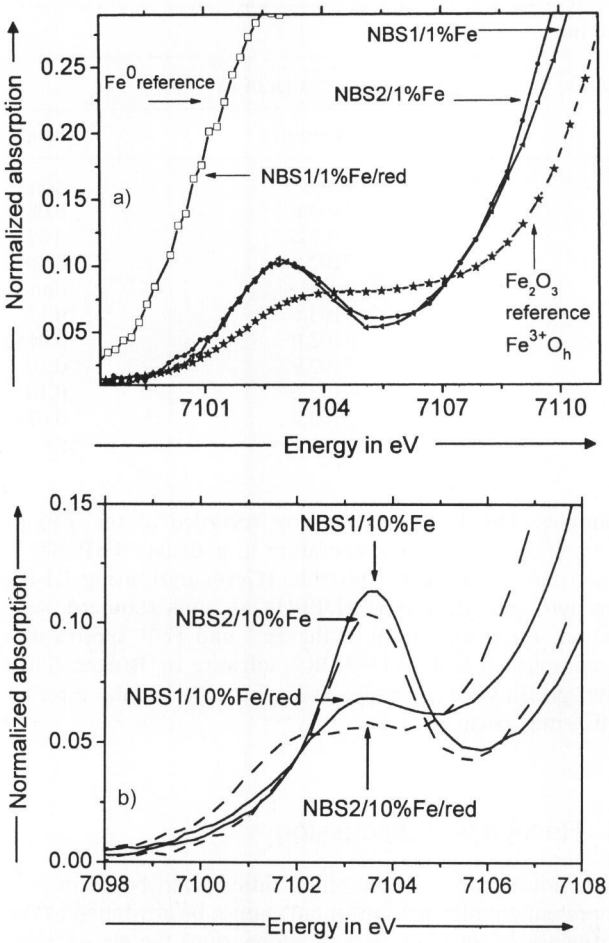

Figures 1a and b. XANES spectra of NBS glasses; doped with a) 1 mol% Fe, b) 10 mol% Fe.

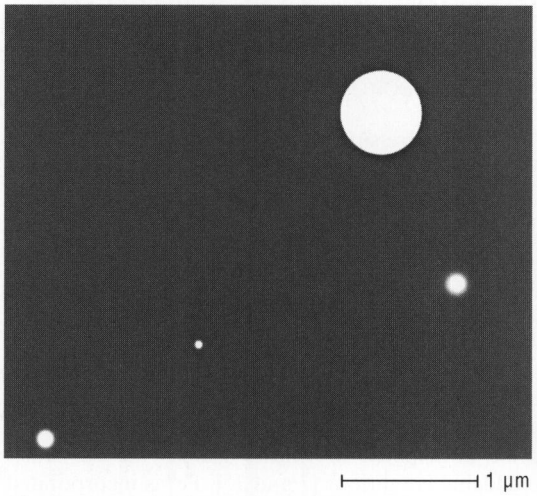

Figure 2. SEM micrograph of NBS1/1% Fe/red.

AFS [16]. In the samples melted under reducing conditions, NBS1/10% Fe/red and NBS2/10% Fe/red, the redox ratio is shifted to Fe^{2+} (table 2, figure 1b). The main edge energy of NBS2/10% Fe is the same as that of the Fe_3O_4 reference, which could indicate the presence of magnetite, a clustered formation that might occur in NBS2 which lacks nonbridging oxygens.

Pre-edge peaks result from forbidden electronic transitions that become partly allowed if ligand orbitals overlap with the species investigated [17]. XANES pre-peaks were used to estimate coordination numbers. For all glass samples the pre-peak heights differ significantly from those of the references included in table 2 and figure 1a. Apparently, the amount of tetrahedral coordination for the measured samples, as indicated by the lowest pre-edge position, is highest in NBS1/10% Fe and decreases in the order NBS2/10% Fe to NBS1/10% Fe/red and NBS2/10% Fe/red (figure 1b). The decreasing amount of tetrahedra scales directly with the decreasing Fe^{3+} / Fe^{2+} ratio deduced from EXAFS analysis. Hence, a large part of Fe^{3+} is tetrahedrally coordinated and Fe^{2+} is mostly in octahedral coordination.

As the Fe^{2+} proportion increases, in reduced melted samples, a broad band emerges in the XANES spectra instead of a disappearing pre-edge peak. This is an indication that the Fe^{2+} octahedra possess a very distorted geometry.

3.1.2 Mössbauer spectroscopy

An Fe concentration of 1 mol% was too low for ^{57}Fe Mössbauer measurements, thus, only samples with 10 mol% were analysed. In the ^{57}Fe Mössbauer spectrum of NBS1/10% Fe isomer shifts are 0.93 (Fe^{2+}) and 0.25 (Fe^{3+}) mm/s relative to α-iron and quadrupole splittings of 2.28 and 0.93 mm/s were calculated (figure 3a). In the corresponding reduced glass NBS1/10% Fe/red the spectrum (figure 3c) is characterized by two superimposed quadrupole doublets centred at 0.98 (Fe^{2+}) and 0.24 (Fe^{3+}) mm/s and corresponding quadrupole splittings of 2.12 and 0.93 mm/s. The spectrum of NBS2/10% Fe (figure 3b) bears two dominant sextets with isomer shifts of 0.31, 0.83, −0.16 and 2.40 mm/s and quadrupole splittings of −0.05 and −0.10 mm/s. In the spectra of NBS2/10% Fe/red (figure 3d) isomer shifts of 1.0 (Fe^{2+}), 0.34 (Fe^{3+}) and 0.91 (Fe^{2+}) mm/s were found. Values for quadrupole splittings are 2.38, 0.7 and 1.93 mm/s.

^{57}Fe Mössbauer spectra in figures 3a, b and c illustrate the strong difference in the solubility of iron in the two glass systems. The spectrum of NBS2/10% Fe (figure 3b) reveals two superimposed dominant sextets, ascribed to Fe^{3+} tetrahedra and mixed valent Fe^{3+} / Fe^{2+} octahedral, both in a segregated magnetite phase [5]. Since the nonbridging oxygens in NBS1 glass enhance the solubility of polyvalent elements in the glass matrix, the formation of clusters, due to a low Fe solubility, occurs only in NBS2 glass [4]. In addition to these sextets a minor component between −3 and 3 mm/s reveals also a small amount of dissolved Fe ions, which are mostly present in the divalent form [5]. Therefore, the sample contains a slightly lower Fe^{3+} / Fe^{2+} ratio than magnetite. No magnetic ordering is observed in the reduced NBS2/10% Fe (figure 3d), only strong Fe^{2+} signals and a weak Fe^{3+} pair. Possibly, a deficiency of Fe^{3+} hinders the formation of Fe^{3+}-Fe^{2+} pairs, therefore those sextets as in NBS2/10% Fe (figure 3b) are not observed.

Use is made of low temperature (4 K) spectra to derive area percentages of each signal. The redox ratios calculated for the samples yield 20 % of Fe^{2+} in NBS1/10% Fe and 30 % of Fe^{2+} in NBS1/10%Fe/red. The remaining percentages are Fe^{3+}. In the reduced NBS2 sample (figure 3d) large amounts (approximately 70 %) of Fe^{2+} were found. Isomer shifts and quadrupole splittings in NBS1 glass are attri-

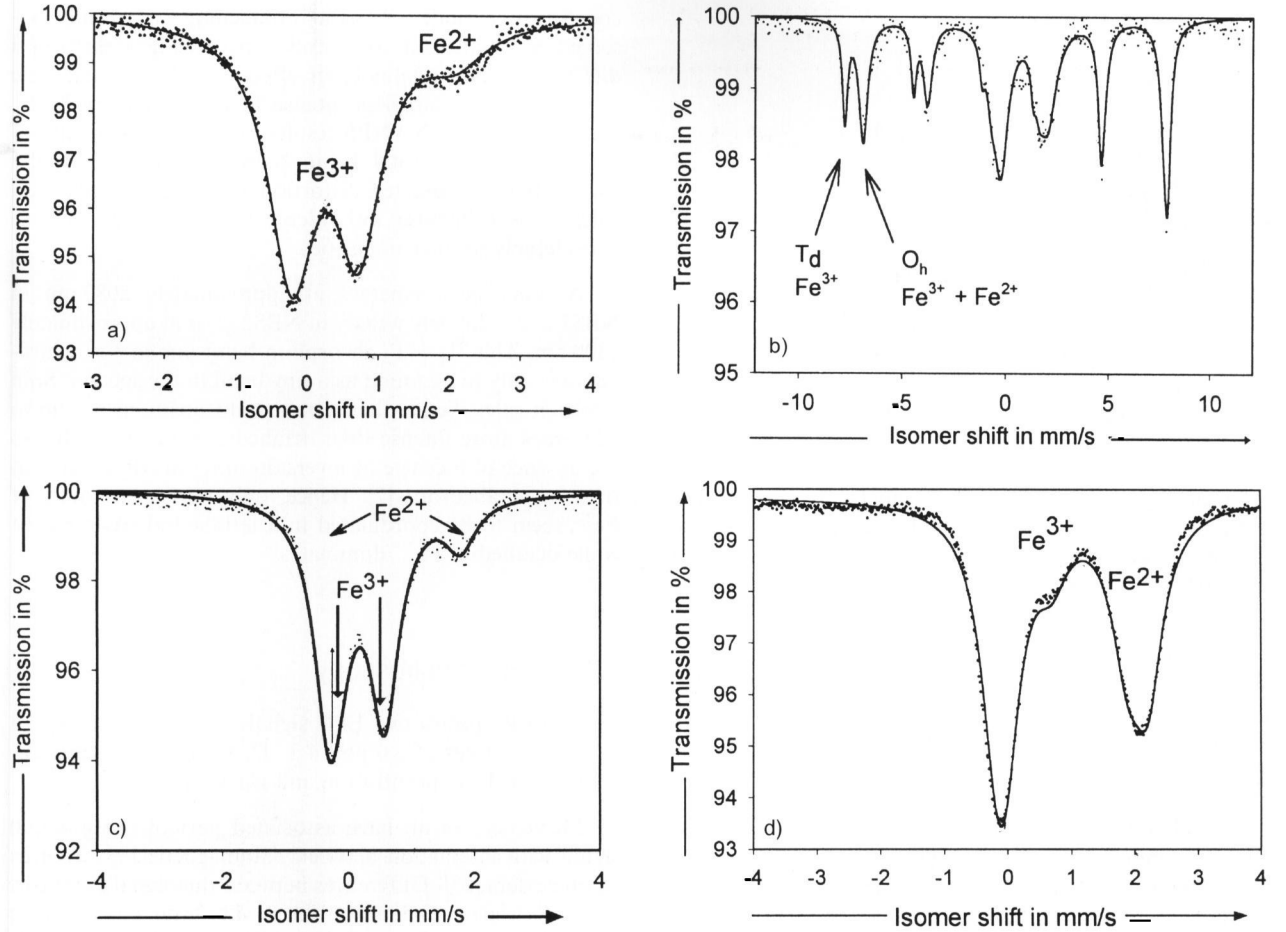

Figures 3a to d. ^{57}Fe Mössbauer spectra at 300 K of a) NBS1/10% Fe, b) NBS2/10% Fe, c) NBS1/10% Fe/red, and d) NBS2/10% Fe/red.

buted to Fe^{2+} in a distorted octahedron and Fe^{3+} ions in tetrahedral coordination both homogeneously distributed in the glass matrix [18].

The full widths at half maximum (FWHM) are 0.7 mm/s for the Fe^{3+} lines and 1 mm/s for the Fe^{2+} lines. Since the line widths of all doublets are large, both Fe^{3+} and Fe^{2+} should be found in more than one coordination mode. The large values for Fe^{3+} quadrupole splittings point to a non-symmetric arrangement of ligands around the ion [5].

3.1.3 Optical absorption spectroscopy

When comparing the spectra of NBS1/1% Fe and NBS2/1% Fe (figure 4) it is seen that Fe absorbs strongly in NBS2 glass over the whole UV and VIS spectral region, whereas Fe absorption is much lower in NBS1 glass. A lack of non-bridging oxygens as in NBS2 glass prohibits the dissolution of high Fe concentrations and thus leads to a clustered formation of Fe^{2+} and Fe^{3+}. Clusters become manifest in direct $Fe^{2+} \rightarrow Fe^{3+}$ intervalence charge transfer (IVCT) transitions with a maximum at approximately 400 nm. IVCT transitions have extremely large extinction coefficients. Only a few ppm of Fe^{2+} and Fe^{3+} in octahedral oxygen coordination and in close proximity (figure 5) — similar to the one in magnetite – cause a deep yellow-brownish to black colouring of the glass. Quenching the NBS2/1% Fe melt

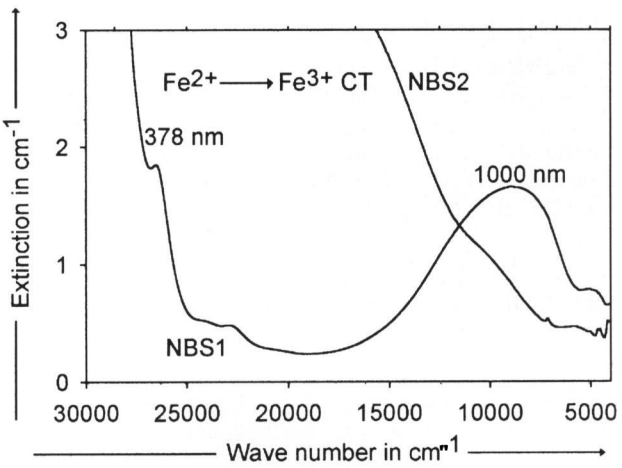

Figure 4. Optical absorption in NBS1/1% Fe and NBS2/1% Fe.

between copper plates diminished the proportion of $Fe^{2+} \rightarrow Fe^{3+}$ IVCT, freezing in a state of more homogeneous distribution of the Fe ions, which dissolve at the high melting temperatures and only cluster upon cooling and glass formation. IVCT transitions are not observed in NBS1 glass. Thus, the optical spectra show a higher capacity for the dissolution of polyvalent ions in the glass matrix of NBS1 glass where many nonbridging oxygens offer preferable bonding sites.

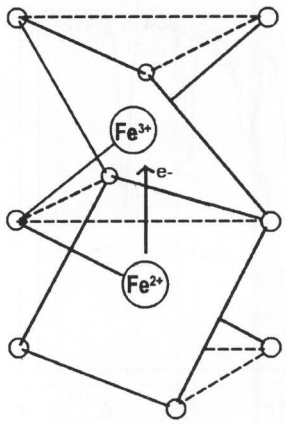

Figure 5. Supposed structure for $Fe^{2+} \rightarrow Fe^{3+}$ intervalence charge transfer (IVCT).

Seven d→d transitions of Fe^{3+} and Fe^{2+} appear in the visible and near IR spectral region. The assignments in table 3 are made according to Kurkjian and Sigety [19]. d→d transitions of Fe^{3+} are spin forbidden and those of Fe^{2+} are Laporte forbidden, hence, their intensities are low [20].

The transitions of tetrahedrally and octahedrally coordinated Fe^{3+} occur at similar energies and cannot be distinguished, but those belonging to tetrahedral Fe^{3+} are more intensive [21]. XANES results indicate that some Fe^{3+} must be tetrahedrally coordinated. Therefore, the observed bands in NBS1 glass (in table 3) are attributed to Fe^{3+} in tetrahedral coordination. The IVCT transitions mentioned above obscure the Fe^{3+} d→d transitions in NBS2 glass and render a direct comparison of Fe^{3+} intensities unfeasible (figure 4). To compare the energies of the transitions in NBS1 and NBS2 glass in spite of IVCT transitions, those at lower Fe concentrations in NBS2 are listed in table 3. No significant differences in the energy positions of the Fe^{3+} transitions are found when NBS1 is compared to NBS2 glass. This could mean the dissolved Fe^{3+} ions occupy similar sites in both matrices.

In the near IR a broad absorption due to Fe^{2+} in octahedral coordination occurs at 1100 nm. This absorption of the $^5T_2 \rightarrow {}^5E$ electronic transition of Fe^{2+} in octahedral coordination is very broad and may be divided into two to three bands. These bands are less structured and broader in NBS1 glass, which denotes a larger variety of possible coordination modes. A band broadening is typically observed in octahedral complexes experiencing a distortion due to a dynamic Jahn-Teller effect [22]. It is remarkable that these bands are less intense in NBS2 than in NBS1 glass even though XANES results suggest a higher ratio of octahedral Fe^{2+} / total Fe in NBS2 compared to NBS1 glass. However, greater distortion often relaxes selection rules, thus otherwise forbidden transitions may increase considerably in their intensities.

Another peak emerges at approximately 2080 nm in NBS1 and extremely weakly in NBS2 glass at approximately 1800 nm. This $^5E \rightarrow {}^5T_2$ absorption band due to Fe^{2+} tetrahedra is only to be found as a tiny band in the spectra. Spin selection rules dictate that tetrahedral transitions are up to 100 times more intense than octahedral transitions, due to the absence of a centre of inversion in tetrahedrons in contrast to octahedrons [7]. Hence, only minute amounts of Fe^{2+} seem to be coordinated in a tetrahedral environment while octahedral Fe^{2+} dominates.

3.1.4 EPR spectroscopy

In the EPR spectra two EPR signals occur at the expected effective g-values of 2.0 and 4.3. Their intensities vary, depending on Fe concentration and glass type.

Montenero et al. have associated part of the $g = 2.0$ signal with interaction between paramagnetic Fe^{3+} centres as in clusters [23]. Differences between this signal's intensities in both glasses were not observed. Clusters as found in the optical absorption spectra should be small at Fe concentrations of 1 mol%, and EPR spectroscopy is less sensitive to their presence than optical absorption spectroscopy to the IVCT absorption.

Different approaches were used for calculating Fe^{3+} concentrations from the signal areas of the EPR spectra. Integration of the normalized peak at $g = 2.0$ usually allows the estimation of the concentration of Fe^{3+}. Because it is a high spin ion, the concentration of Fe^{3+} in the glasses investigated was found to be not proportional to the area of the integrated peak at $g = 2.0$ [24]. Fe^{3+} contents can, however, be evaluated as described by Elvers [25]. The calcu-

Table 3. Transitions of Fe ions in the glasses studied (fits at 1 mol% are listed)

species	transition	NBS1			NBS2		
		wavelength in nm	FWHM[1] in cm^{-1}	E / d in cm^{-1}	wavelength in nm	FWHM[1] in cm^{-1}	E / d in cm^{-1}
Fe^{3+} T_d	$^6A_1 \rightarrow {}^4T_2(D)$	378	1600	1.6	375[2]	3300[2]	super-
Fe^{3+} T_d/O_h	$^6A_1 \rightarrow {}^4E^4A_1$	408	2000	0.5	415[2]	2200[2]	posed
Fe^{3+} T_d/O_h	$^6A_1 \rightarrow {}^4E^4A_1$	438	1900	0.3	441[2]	2500[2]	by
Fe^{3+} T_d/O_h	$^6A_1 \rightarrow {}^4T_2$	485	3700	0.2	490[2]	5600[2]	IVCT[3]
Fe^{3+} T_d/O_h	$^6A_1 \rightarrow {}^4T_1$	600	4100	0.2	640[2]	5600[2]	
Fe^{2+} O_h	$^5T_2 \rightarrow {}^5E$	815	4600	0.9	860	3500	0.3
		1110	4000	1.4	1100	3300	0.5
		1365	1900	0.5	1500	2800	0.1
$Fe^{2+}T_d$	$^5E \rightarrow {}^5T_2$	2080	3000	0.7	1800	3500	0.2

[1] FWHM: full width at half maximum.
[2] Energy positions and FWHM derived from spectra of 0.1 mol% Fe.
[3] IVCT = Intervalence charge transfer.

lated Fe^{3+} values of 80 and 70 ± 10 % confirmed the Fe^{3+} percentages from XANES of 80 and 60 ± 5 % Fe^{3+} in the samples NBS1/1%Fe and NBS2/1%Fe, respectively.

The ratio $I_{g=2.0}$ / $I_{g=4.3}$ could yield information on the coordination of Fe^{3+} ions. The g = 2.0 signal has been assigned to spin-spin interactions as they occur in clustered Fe^{3+} whereas the signal with an effective g-value of 4.3 is ascribed to Fe^{3+} in tetrahedral coordination with C_{2v} symmetry [23, 25 and 27]. The different coordination behaviour of Fe^{3+} observed with optical absorption spectroscopy and EXAFS/XANES should result in varied $I_{g=2.0}$ / $I_{g=4.3}$ ratios. However, the measured $I_{g=2.0}$ / $I_{g=4.3}$ ratios deviate and unfortunately no unambiguous results concerning the Fe^{3+} coordination could be derived from EPR spectra with their large error margins.

3.1.5 SEM / TEM studies

Energy dispersive X-ray analysis measurements have detected Fe^0 particles of up to 0.64 µm in sample NBS1/1% Fe/red (figure 2).

Glasses with an Fe content of 10 mol% or more show a great tendency towards crystallization because of the high field strength of the Fe ions. NBS2 glasses with 10 mol% Fe showed phase separation, which could be verified by transmission electron microscope measurements of etched samples. The dissolved iron is expected to be contained within the sodium borate phase [5] and the resulting magnetic ordering was indeed shown by Mössbauer spectroscopy.

3.2 Valence states of antimony – Sb^{5+} ($4d^{10}$) / Sb^{3+} ($4d^{10}$ $5s^2$) / Sb^0 ($4d^{10}$ $5s^2$ $5p^3$)

3.2.1 XANES spectroscopy

Both XANES L_I-edge positions of glasses with 1 mol% Sb are at 4698 eV. This compares well to 4702.3 eV for Sb_2O_3 that was measured for reference purposes. Most antimony is in the oxidation state +3 in both glass types [17].

In the XANES spectra, no pre-peak is observed. The L_I-edge position yields information on the Sb valence only. Unfortunately, EXAFS oscillations are too weak to deduce any information on the coordination behaviour of Sb^{3+}.

3.2.2 Mössbauer spectroscopy

The isomer shifts in the ^{121}Sb Mössbauer spectra differ slightly for the glasses (figure 6). Measured values are (−12.21 ± 0.05) mm/s in NBS1/1% Sb and (−11.60 ± 0.05) mm/s for NBS2/1% Sb. The quadrupole coupling constants are 16.6 mm/s in NBS1 and 17.9 mm/s in NBS2 glass. Hence, most of the Sb is present as Sb^{3+}. Still, the measured data scatters. From comparison with spectra of glasses containing 6 % of all Sb as Sb^{5+} it can be deduced that the Sb^{5+} content must be below 5 % in the present glasses.

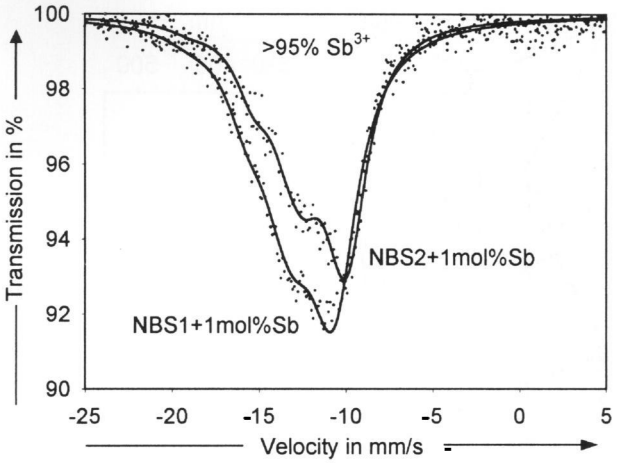

Figure 6. ^{121}Sb Mößbauer spectra of NBS1/1% Sb and NBS2/1% Sb.

A loss of 5 s-electron density in the valence band can be detected from the ^{121}Sb Mössbauer isomer shifts [28]. An increasing isomer shift represents an increasing s-electron density at the Sb nucleus. The varying isomer shifts in the presented ^{121}Sb Mössbauer spectra suggest that the s-electron density at the Sb^{3+} nucleus is somewhat higher in the NBS1 than in the NBS2 glass matrix, which agrees well with the higher optical basicity (electron donor power) of the NBS1 glass.

A line broadening is typically observed in glasses, where structures are more distorted than in crystals. Quadrupole splittings emerge if the investigated isotopes diverge from cubic symmetry.

3.2.3 Optical absorption spectra

Only an edge shift is observed in the optical absorption spectra of the two Sb doped samples (figure 7a). In samples NBS1/1% Sb and NBS2/1% Sb, the absorption edge (Eld = 1 cm^{-1}) is found at 300 and 275 nm, respectively. The intensity of the absorbance observed due to Sb^{3+} is too high for further analysis.

The wavelengths of the electronic d→s transitions of Sb^{5+} are positioned in the VUV spectral region and could not be studied because of the high absorption due to Sb^{3+} [2].

3.2.4 Photoluminescence spectroscopy

Sb^{3+} fluoresces in both glass types (figure 7b). Since Sb^{3+} ions prevail in the doped glasses, the photoluminescence spectra are assigned to the Sb^{3+} optically active ions [3 and 29]. The fluorescence intensity is drastically higher in NBS1 than in NBS2 glass, which might be related to a significant concentration quenching. Concentration quenching in NBS2 glass could be a consequence of lacking nonbridging oxygens and subsequent clustering of Sb^{3+}. Similar observations as for NBS1 and NBS2 glass were made in the case of the technical glasses Duran® and BK7®, doped with Sb^{3+} [3]. Another possible explanation would be that since the absorption at the excitation wavelength is larger for

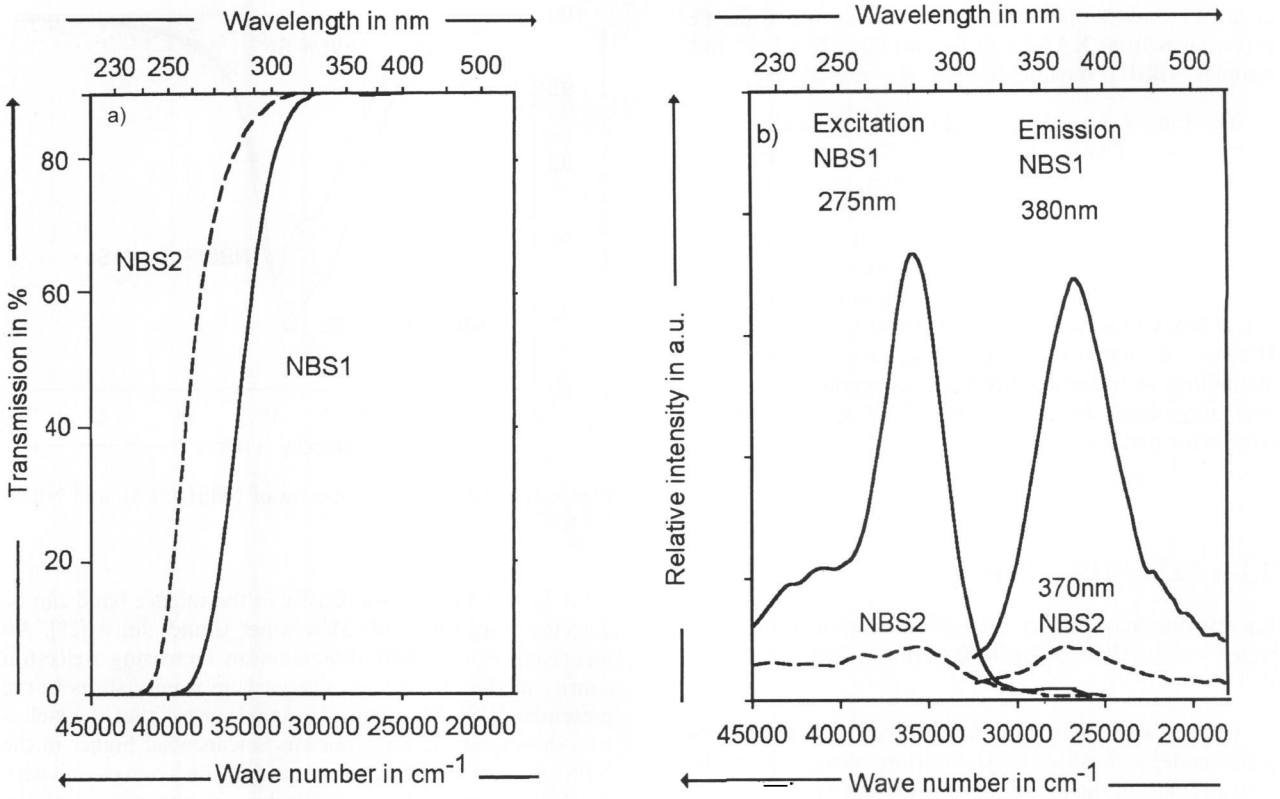

Figures 7a and b. Optical spectra of NBS1/1% Sb and NBS2/1% Sb, a) transmission d = 10 mm, and b) fluorescence.

NBS1/1% Sb than for the NBS2 samples, more photons will be absorbed in NBS1 glass (figures 7a and b).

The emission maximum is found at approximately 380 nm in NBS1 and at 370 nm in NBS2 glass. One broad emission band is linked to one excitation band, even at lower Sb concentrations. A Jahn-Teller distortion may, under certain circumstances, induce the emergence of two emissions [30]. This could explain the wide and asymmetric fluorescence emission for both NBS1 and NBS2 glass, especially as the observed structure of excitation is also due to a dynamic Jahn-Teller effect [31].

3.2.5 SEM studies

Sb^0 spheres were found in NBS2/1% Sb as analysed by SEM with EDX. In NBS1 glass with its higher optical basicity and its nonbridging oxygens all Sb dissolved readily.

3.3 Valence states of titanium – Ti^{4+} ($3d^0$)/Ti^{3+} ($3d^1$)

3.3.1 XANES spectroscopy

Measured XANES spectra are displayed in figure 8. The edge energies are 4979.0 and 4978.3 eV for NBS1/1% Ti and NBS2/1% Ti, respectively. These energies compare well to those of TiO_2 (as anatase, figure 8). Such small changes in the edge energies stand for very limited alterations of the redox ratio. Ti is built into the NBS glass matrices predominantly as Ti^{4+}.

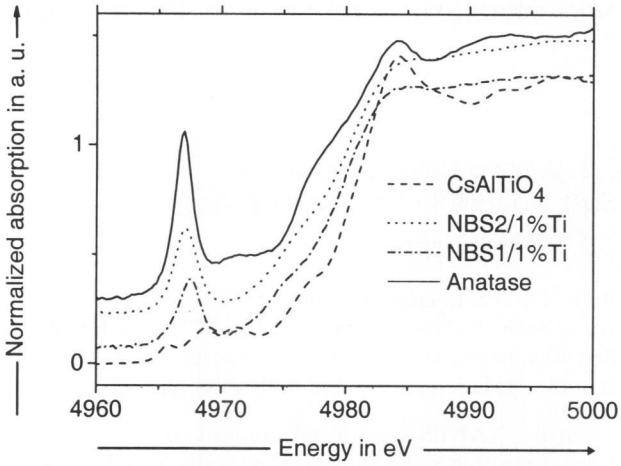

Figure 8. XANES spectra of NBS1/1% Ti, NBS2/1% Ti, and reference substances.

The addition of graphite powder to the melt induced a partial reduction of Ti^{4+} ions to Ti^{3+}. The edge energy of NBS1/1% Ti/red is 4978.1 eV and lower than the edge energy of the corresponding sample without graphite, NBS1/1% Ti.

Ti^{4+} is incorporated into the NBS glass matrix in four- five- and sixfold coordination. To evaluate the predominant coordination number in each sample reference substances of known coordination modes were measured [16]. Criteria for comparison were the position of each pre-peak along with its relative intensity. Ti^{4+} references with fourfold coordination show energy positions of the pre-peak between

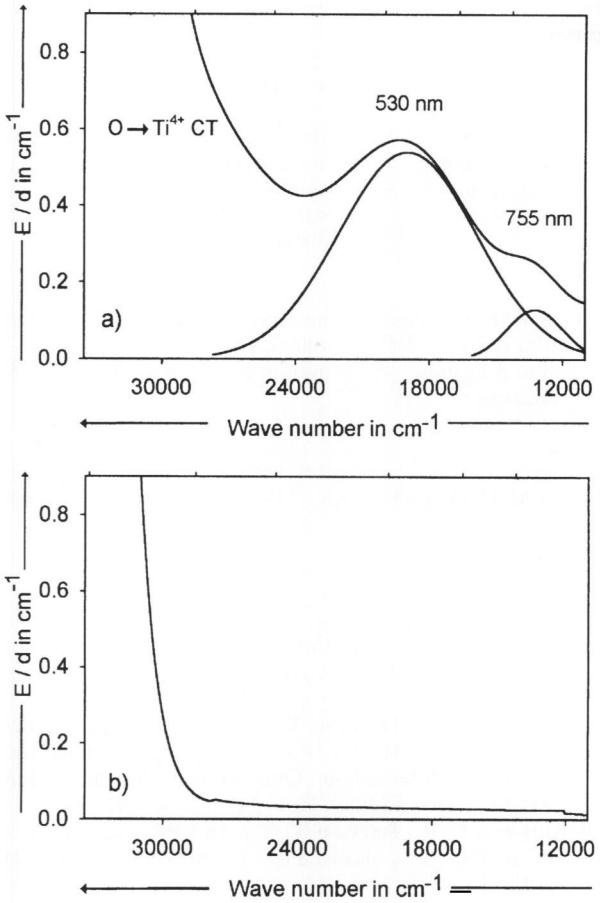

Figures 9a and b. UV-VIS absorption in a) NBS1/1% Ti/red, and b) NBS1/1% Ti.

4969.25 and 4969.8 eV and pre-peak relative intensities between 0.45 and 0.77. For Ti^{4+} complexes with fivefold coordination energies between 4970.3 and 4970.7 eV and relative intensities of 0.30 and 0.62 were measured. Heights of the pre-edge features in the nonreduced samples were 0.31 and 0.46 a.u. (NBS1) and 0.28 and 0.41 a.u. (NBS2). In this way it was shown that Ti^{4+} has an average coordination number of five in NBS2 glass whereas the average number of ligands in NBS1 glass is somewhat lower and closer to four.

3.3.2 Optical absorption spectra

The UV region of the optical Ti spectra is dominated by charge transfer transitions between 240 and 190 nm with high extinction coefficients. Absorption edges (E/d = 1 cm^{-1}) are found at 322 nm for NBS1/1% Ti and 325 nm for NBS2/1% Ti.

Since large proportions of Ti are in oxidation state +4, the absorption is ascribed to O → Ti^{4+} charge transfer transitions. Their intensities are too high for further analysis.

Figures 9a and b show the absorption of Ti^{3+} in NBS1/1% Ti/red and NBS1/1% Ti. A very broad peak was observed at 530 nm (and a weaker one at 755 nm). Ti^{3+} coordinates as an octahedron and experiences a heavy distortion due to a dynamic Jahn-Teller effect [7]. This was observed in all UV-VIS-near IR spectra of the Ti^{3+} containing NBS samples.

3.3.3 Photoluminescence spectroscopy

Ti^{4+} shows photoluminescence in both glasses with an emission maximum at 480 to 500 nm and an excitation maximum at 260 and 290 nm (NBS1 and NBS2 glass, respectively). The intensity is higher in NBS1 glass. Due to the high field strength of Ti^{4+}, a clustered formation at higher concentrations is likely, at least in NBS2 glass where the lack of nonbridging oxygens favours this effect. Thus, the energy migration between clustered Ti^{4+} ions should be easier. The fact that only one emission maximum was observed for all NBS samples leads to the assumption that only one of the differently coordinated Ti^{4+} species (which have already been discussed with the XANES results) fluoresces.

3.3.4 EPR spectroscopy

Only when the rate of Ti reduction was significant, signals with effective g-values of 1.93 appeared and could be attributed to Ti^{3+} in octahedral coordination. According to the EPR spectra no more than 10 % of the total Ti could be reduced to Ti^{3+}. Other glasses had signals of negligible intensities, thus Ti^{3+} contents were ≤ 0.01 mol%.

According to Schlick et al., Ti^{3+} – Ti^{3+} coupling might be seen in the EPR spectra as well [32]. Although no such signal was observed for the NBS samples, the existence of such dimers cannot be ruled out, since glasses often show lower sensitivities to paramagnetic species than crystals [33].

4. Conclusions

Important results of the different measuring techniques are summarized in table 4.

It was shown for the two borosilicate glasses which both contained 74 mol% SiO_2 that the presence of nonbridging oxygens in NBS1 glass increases the solubility of the polyvalent ions Fe^{3+}, Fe^{2+} and Sb^{3+} and possibly of Ti^{4+}. Cluster formation occurs only in NBS2 glass, which lacks nonbridging oxygens. These clusters can result in lowered UV and VIS transmission, as seen for the IVCT between Fe^{2+}→Fe^{3+}. The optical basicities of the glasses seem to influence the coordination behaviour of Ti^{4+} and Fe^{3+}. Average coordination numbers are lower in the high alkaline glass matrix of NBS1 glass.

A varying matrix influence was detected for the Fe, Ti and Sb ions investigated. For Fe and Ti ions, the matrix seems to offer more different coordination sites than for Sb^{3+} ions. Fe^{3+} can be built in both in octahedral and tetrahedral coordination. Fe^{2+} is coordinated mostly octahedrally and exhibits a strong Jahn-Teller distortion. Ti is incorporated as Ti^{4+} in four-, five- and sixfold coordination, into both glasses. The average coordination number is slightly lower in NBS1 than in NBS2 glass. Minor amounts of Ti^{3+} could only be formed when strongly reducing melting conditions were applied. Just the opposite is true for Sb, where the oxidation of Sb^{3+} to Sb^{5+} could not be observed. The coordination of Sb^{3+} seems to be similar in both glass types, only the amount of distortion varies. Sb^{3+} has probably a preferred coordination sphere which it will adopt as long as the Sb concentration is low enough.

Table 4. Summary of combined results for different methods and concentrations

sample	x = Fe	x = Sb	x = Ti
	80 % Fe^{3+}, 20 % Fe^{2+} [1) 5)]	100 % Sb^{3+} [1) 2) 4)]	100 % Ti^{4+} [1) 3) 4) 5)]
NBS1/1x%	Fe^{3+} T_d ($+O_h$) [1) 3) 5)]	4 to 5 ligands,	average coordination
	Fe^{2+} O_h ($>>T_d$) [3)]	distortion[2)]	number ≤ 5
NBS1/1x%/red	Fe^0 [1) 6)]	–	<10 % Ti^{3+} [5)]
			distorted octahedron [1) 3)]
NBS1/10x%	$\geq$80 % Fe^{3+}, $\leq$20 % Fe^{2+} [1) 2)]	=	–
NBS1/10x%/red	70% Fe^{3+} 30% Fe^{2+} [2)]	=	–
	cluster formation [3)] IVCT [7)]	low Sb solubility[4) 6)]	inhomogeneous site distribution[4)]
NBS2/1x%	60% Fe^{3+}, 40% Fe^{2+} [1)]	100 % Sb^{3+} [1) 2) 4)]	100 % Ti^{4+} [1) 3) 4) 5)]
	$Fe^{3+}T_d+O_h$ [1) 5)]	4 to 5 ligands,	average coordination number ≥ 5
	$Fe^{2+}O_h$ ($>>T_d$) [3)]	distortion[2)]	
NBS2/10x%	cluster formation, magnetic ordering [1) 2) 3)]	=	=
NBS2/10x%/red	70 to 100 % Fe^{2+}, mostly distorted octahedron [1) 2) 3)]	–	=

[1)] XANES, [2)] Mössbauer, [3)] optical absorption, [4)] fluorescence, [5)] EPR, [6)] SEM/TEM spectroscopy, [7)] IVCT = Intervalence charge transfer.

This multi-method approach did not only help to verify results from the different analytical tools employed, but also resulted in a much more complete information of all kinds of structural aspects, including the redox ratio, the coordination and site distribution of the dopants, than any of the spectroscopic methods could have detected alone. At higher concentration the methods XANES and Mössbauer spectroscopy were used to determine redox ratios and the average coordination numbers. Optical spectroscopy and fluorescence are more sensitive to small changes in coordination behaviour and to cluster effects. EPR spectroscopy could show clustering effects (e.g. for Fe), but can also be used to calculate the concentration of paramagnetic species as Ti^{3+}.

*

The authors would like to thank SCHOTT JENA^{er} Glas Stiftungsfonds for their financial support. We are grateful to M. Friedrich of the Institute of Inorganic and Analytical Chemistry for carrying out the EPR measurements and to G. Völksch for electron microscopy analysis. We would like to thank R. Keding for supplying Ti references for XANES measurements.

5. References

[1] Ehrt, D.; Reiß, H.; Vogel, W.: Mikrostrukturuntersuchungen an CoO-haltigen NaO_2-B_2O_3-SiO_2-Gläsern. Silikattechnik **28** (1977) no. 12, pp. 359–364.

[2] Duffy, J. A.: Bonding, energy levels and bands in inorganic solids. Harlow: Longman Scientific Technical, 1990.

[3] Ehrt, D.; Ebeling, P.: Radiation defects in borosilicate glasses. Glass Technol. **44** (2003) no. 2, pp. 46–49.

[4] Möncke, D.; Ehrt, D.; Eckert, H. et al.: Influence of melting and annealing conditions on the structure of borosilicate glasses. Phys. Chem. Glasses **44** (2003) no. 2, pp. 113–116.

[5] Ehrt, D.; Reiß, H.; Vogel, W.: Einbau und Verteilung von Fe_2O_3 auf die Mikrophasen in Grundgläsern des Systems NaO_2-B_2O_3-SiO_2. Silikattechnik **27** (1976) no. 9, pp. 304–309.

[6] Iwatomo, N.; Umesaki, N.; Hidako, H. et al.: Structure of glasses and melts in the Na_2O-SiO_2-TiO_2 system. (Orig. Jpn.) J. Ceram. Soc. Jpn. **94** (1986) pp. 856–862.

[7] Johnston, W. D.: Oxidation-reduction equilibria in iron-containing glass. J. Am. Ceram. Soc. **47** (1964) no. 4, pp. 198–201.

[8] Schütz, A.; Ehrt, D.; Yang, X. et al.: Spectroscopic characterisation of Fe-, Sb-, Sn-, Pb- and Ti-complexes in glasses. In: Proc. 7th International Otto Schott Colloquium, Jena 2002. Glass Sci. Technol. **75 C 2** (2002) pp. 442–445.

[9] Kurkjian, C. R.; Peterson, G. E.: An EPR-study of Ti^{3+}-Ti^{4+} in TiO_2-SiO_2 glasses. Phys. Chem. Glasses **15** (1974) pp. 12–17.

[10] Farges, F.; Brown, G. E. Jr.: Coordination chemistry of titanium (IV) in silicate glasses and melts: IV. XANES studies of synthetic and natural volcanic glasses and tektites at ambient temperature and pressure. Geochim. Cosmo. Acta **61** (1997) no. 9, pp. 1863–1870.

[11] Mosel, B. D.; Müller-Warmuth, W.; Stahlberg, B.: Combined electrochemical and Mössbauer studies of the Sb^{3+}/Sb^{5+} equilibrium in a silicate glass-forming melt. Glastech. Ber. **61** (1988) no. 12, pp. 335–340.

[12] Leister, M.; Ehrt, D.: Redox behavior of iron and vanadium ions in silicate melts at temperatures up to 2000 °C. Glastech. Ber. Glass Sci. Technol. **72** (1999) no. 5, pp. 153–160.

[13] Möncke, D.; Ehrt, D.: Influence of melting and annealing conditions on the optical spectra of a borosilicate glass doped with CoO and NiO. Glastech. Ber. Glass Sci. Technol. **75** (2002) no. 4, pp. 163–173.

[14] Du, W. F.; Kuraoka, K.; Akai, T. et al.: Study of Al_2O_3 effect on structural change and phase separation in Na_2O-B_2O_3-SiO_2 glass by NMR. J. Mat. Sci. **35** (2000) no. 19, pp. 4865–4871.

[15] Ehrt, D.; Leister, M.; Matthai, A.: Polyvalent elements iron, tin and titanium in silicate, phosphate and fluoride glasses and melts. Phys. Chem. Glasses **42** (2001) no. 3, pp. 231–239.

[16] Yang, X. C.; Dubiel, M.; Schütz, A. et al.: An investigation of valence state and structural environment of polyvalent Fe and Ti ions in glasses by X-ray absorption spectroscopy. Phys. Chem. Glasses. Accepted for publication.

[17] Dubiel, M.; Yang, X.; Schütz, A. et al.: Eisen- und Titanstrukturgruppen in Natriumborosilicatgläsern. In: Ext. Abstr. 77. Glastechnische Tagung, Wernigerode, Leipzig 2003. Offenbach: Deutsche Glastechnische Gesellschaft, 2003.

[18] Dyar, M. D.: A review of Mössbauer data on inorganic glasses: the effects of composition on iron valency and coordination. Am. Miner. **70** (1985) pp. 304–316.

[19] Kurkjian, C. R.; Sigety, E. A.: Co-ordination of Fe^{3+} in glass. Phys. Chem. Glasses **9** (1968) no. 3, pp. 73–83.
[20] Schäfer, H. L.; Glieman, G.: Einführung in die Ligandenfeldtheorie. Leipzig: Geest und Portig, 1967.
[21] Fenstermacher, J. E.: Optical absorption due to tetrahedral and octahedral ferric iron in silicate glasses. J. Non. Cryst. Sol. **38**, **39** (1980) pp. 239–244.
[22] Cotton, F. A.; Meyers, M. D.: Magnetic and spectral properties of the spin-free $3d^6$ systems iron(II) and cobalt(III) in cobalt(III)hexafluoride ion: Probable observation of dynamic Jahn-Teller effect. J. Am. Chem. Soc. **82** (1960) pp. 5023–5026.
[23] Montenero, A.; Friggeri, M.; Giori, D. C. et al.: Iron-soda-silica glasses: preparation, properties, structure. J. Non. Cryst. Sol. **84** (1986) pp. 45–60.
[24] Electron paramagnetic resonance of d transition metal compounds. New York: Elsevier, 1992.
[25] Elvers, A.; Weißmann, R.: ESR spectroscopy – an analytical tool for the glass industry. Glastech. Ber. Glass Sci. Technol. **74** (2001) no. 2, pp. 32–38.
[26] Rüssel, C.: Iron oxide-doped alkali-lime-silica glasses. Pt 1. EPR investigations. Glastechn. Ber. **66** (1993) pp. 68–75.
[27] Camara, B.: Einbau von Eisen in Glas. Glastechn. Ber. **51** (1978) pp. 87–95.
[28] Durand, J.-M.; Lippens, P. E. et al.: Sb LIII-edge XAS study of the ternary system Sb_2S_3-As_2S_3-Tl_2S. J. Solid State Chem. **194** (1996) pp. 109–121.
[29] Paje, S. E.; Garcia, M. A.; Villegas, M. A. et al.: Optical properties of silver ion-exchanged antimony doped glass. J. Non. Cryst. Sol. **278** (2000) pp. 128–136.
[30] Oomen, E. W. J. L.; Smit, W. M. A.; Blasse, G.: Jahn-Teller effect in the emission and excitation spectra of the Sb^{3+} ion in LPO_4 (L=Sc, La, Y). Phys. Rev. **B 37**, **1** (1988) pp. 18–26.
[31] Oomen, E. W. J. L.; Smit, W. M. A.; Blasse, G.: Jahn-Teller effect in the Sb^{3+} emission in zircon-structured phosphates. Chem. Phys. Lett. **112** (1984) no. 6, pp. 547–550.
[32] Schlick, S; Alonso-Amigo, M. G.; Binding of paramagnetic ions in ionomers. Soc. Faraday Trans. **1**, **83** (1987) no. 12, pp. 3575–3586.
[33] Griscom, D. L.: Electron spin resonance in glasses. J. Non-Cryst. Sol. **40** (1980) pp. 211–272.

E604P005

Contact:

Doz. Dr. Doris Ehrt
Otto-Schott-Institut für Glaschemie
Friedrich-Schiller-Universität Jena
Fraunhoferstraße 6
D-07743 Jena

E-mail: doris.ehrt@uni-jena.de